MOLECULAR AND CELLULAR BIOLOGY, Sept. 2011, p. 3759–3772 Vol. 31, No. 18
0270-7306/11/$12.00 doi:10.1128/MCB.05243-11

Bioluminescence Imaging Captures the Expression and Dynamics of Endogenous *p21* Promoter Activity in Living Mice and Intact Cells[▽]

Kelsey L. Tinkum,[1,2,3] Luciano Marpegan,[6] Lynn S. White,[1,2,3] Jinwu Sun,[1,2] Erik D. Herzog,[6] David Piwnica-Worms,[1,2,3,4]* and Helen Piwnica-Worms[1,3,5]*

Department of Cell Biology and Physiology,[1] Molecular Imaging Center, Mallinckrodt Institute of Radiology,[2] BRIGHT Institute,[3] Department of Developmental Biology,[4] and Department of Internal Medicine,[5] Washington University School of Medicine, St. Louis, Missouri 63110, and Department of Biology, Washington University, St. Louis, Missouri 63130[6]

Received 18 February 2011/Returned for modification 23 March 2011/Accepted 13 July 2011

To interrogate endogenous *p21$^{WAF1/CIP1}$* (*p21*) promoter activity under basal conditions and in response to various forms of stress, knock-in imaging reporter mice in which expression of firefly luciferase (*FLuc*) was placed under the control of the endogenous *p21* promoter within the *Cdkn1a* gene locus were generated. Bioluminescence imaging (BLI) of *p21* promoter activity was performed noninvasively and repetitively in mice and in cells derived from these mice. We demonstrated that expression of FLuc accurately reported endogenous *p21* expression at baseline and under conditions of genotoxic stress and that photon flux correlated with mRNA abundance and, therefore, bioluminescence provided a direct readout of *p21* promoter activity *in vivo*. BLI confirmed that p53 was required for activation of the *p21* promoter *in vivo* in response to ionizing radiation. Interestingly, imaging of reporter cells demonstrated that p53 prevents the extracellular signal-regulated kinase/mitogen-activated protein kinase pathway from activating *p21* expression when quiescent cells are stimulated with serum to reenter the cell cycle. In addition, low-light BLI identified *p21* expression in specific regions of individual organs that had not been observed previously. This inducible *p21^{FLuc}* knock-in reporter strain will facilitate imaging studies of p53-dependent and -independent stress responses within the physiological context of the whole animal.

p21$^{Waf1/CIP1}$ (*p21* here) encodes a member of the CIP/KIP family of cyclin-dependent protein kinase (CDK) inhibitors that regulates a variety of complex and sometimes opposing cell processes. One of the best-characterized properties of p21 is its ability to impair cell cycle advancement by binding to and inhibiting CDKs (1). Indeed, *p21* is a transcriptional target of p53 and, in cells experiencing genotoxic stress, is critical for arresting cells in the G_1 phase of the cell division cycle through its binding to CDK2 complexes (35). Furthermore, p21 helps to sustain a G_2 arrest by binding to CDK1 complexes. It has been reported that the extracellular signal-regulated kinase (ERK)/mitogen-activated protein kinase (MAPK) pathway activates *p21* expression in response to serum stimulation (6, 25), but the impact of p53 was not fully characterized. Paradoxically, p21 also positively regulates cell cycle progression by aiding in the assembly of stable CDK4/6-cyclin D complexes (34).

In addition to regulating cell cycle progression, p21 binds to proliferating cell nuclear antigen (PCNA), a DNA polymerase δ processivity factor, thereby blocking processive DNA synthesis (26). Interactions between p21 and PCNA have also been reported to hinder DNA repair (8). p21 can also repress transcription indirectly by inhibiting cyclin-CDK complexes, which in turn prevent phosphorylation of Rb family proteins (34). In addition, p21 can modulate transcription directly by binding to various transcription factors, such as E2F1, STAT3, and MYC (1).

The cytoplasmic pool of p21 has been shown to regulate apoptosis as well as the actin cytoskeleton. p21 inhibits apoptosis by binding to and inhibiting the activity of proteins that induce apoptosis, including procaspase 3, caspases 8 and 10, and the protein kinases SAPK and ASK1. p21 also regulates the actin cytoskeleton by inhibiting ROCK (5, 23). Inhibition of ROCK may also be selected for during tumor progression to enhance cell motility. Indeed, high levels of cytoplasmic p21 have been observed in a number of human cancers and are associated with high-grade tumor types and a poor prognosis (3).

Given the multifaceted and complex functions of p21 *in vivo*, it is not surprising that the *p21* promoter is controlled by a plethora of signaling pathways (epidermal growth factor [EGF], nerve growth factor, transforming growth factor β, gamma interferon, interleukin-6, progesterone, and the Ras/Raf pathways) and transcription factors (p53, SP1/3, AP2, STAT1/3/5, E2F1/3, SMAD3/4, and c/EBPα/β) (1, 14). Northern blot analysis and *in situ* hybridization have been used to examine *p21* expression in various mouse organs *ex vivo* at baseline and following exposure of mice to various forms of genotoxic stress (7, 27, 30). However, there are significant discrepancies among these studies regarding which tissues have high versus low versus undetectable levels of *p21* mRNA as well as the contribution made by p53 to basal expression of *p21*. In particular, the small intestine has been reported to

* Corresponding author. Mailing address for Helen Piwnica-Worms: Washington University School of Medicine, Campus Box 8228, 660 S. Euclid, St. Louis, MO 63110. Phone: (314) 362-6812. Fax: (314) 362-3709. E-mail: hpiwnica@wustl.edu. Mailing address for David Piwnica-Worms: Washington University School of Medicine, Campus Box 8225, 510 S. Kings highway building, St. Louis, MO 63110. Phone: (314) 362-9356. Fax: (314) 362-0152. E-mail: piwnica-wormsd@mir.wustl.edu.

▽ Published ahead of print on 26 July 2011.

show undetectable (38), low (29, 37), moderately high (7, 24), and very high (27) baseline levels of *p21* expression. Because conventional biochemical techniques have limitations in sensitivity and specificity arising from variations in reagent fidelity, specimen preparation, and quantification difficulties in many organs, there is considerable interest in imaging gene expression and signaling pathways noninvasively in their normal physiological context within living organisms (10, 17). With that intent, transgenic reporter mice carrying a *p21 LacZ* transgene (37) as well as a *p21* firefly luciferase (*FLuc*) transgene (29) have been developed and described. However, design strategies limited the output of these reporter strains. For example, both studies used a truncated *p21* promoter to drive reporter expression and therefore eliminated key signaling inputs regulating *p21* promoter activity. In addition, in one case, reporter mice contained 2, 3, or 22 copies of the *p21* transgene and therefore did not accurately report endogenous levels of expression (37).

Therefore, to monitor both p53-dependent and -independent regulation of the endogenous *p21* promoter in the proper context of a vertebrate animal, we generated knock-in reporter mice, in which expression of the *FLuc* gene is placed under the control of the endogenous *p21* promoter. We demonstrate that expression of luciferase accurately reports endogenous *p21* expression at baseline and following ionizing radiation (IR), enabling the activity of the endogenous *p21* promoter to be dynamically monitored in real time *in vivo*, under a variety of experimental conditions. Known functions of p21 were validated noninvasively and in a tissue-specific manner. Imaging of reporter murine embryonic fibroblasts (MEFs) demonstrated that p53 prevents the ERK/MAPK pathway from activating *p21* expression when quiescent cells are stimulated to reenter the cell cycle with serum, while imaging of reporter mice revealed novel sites of high-level *p21* expression.

MATERIALS AND METHODS

This study was carried out in strict accordance with the recommendations in the *Guide for the Care and Use of Laboratory Animals* of the National Research Council (28). The Committee on the Ethics of Animal Experiments at Washington University approved all animal protocols used in the study.

Construction of the *p21*-targeting vector. PCR was used to amplify 129/SvJ genomic DNA encoding *p21* (Invitrogen). The 5′-targeting arm was generated using primers 5′-GAT CCC CGG TCC TTG TGA A-3′ and 5′-CCA TGG TGC CTG TGG CTG AAA C-3′. This amplified 4.0 kb of *p21* genomic DNA beginning within intron 1 and ending in exon 2 just after the start codon. The primer design inserted an NcoI site within the ATG start codon in exon 2. The 3′-targeting arm was generated using primers 5′-TGT CCG ACC TGT TCC GCA CAG-3′ and 5′-GGT AAG ACC AGG GAA TCC CAC-3′. This amplified 1.8 kb of *p21* genomic DNA extending from within exon 2 to noncoding sequences downstream of exon 3. PCR products were inserted into the Topo TA vector (Invitrogen). A BamHI/NcoI fragment encoding the 5′-targeting arm was then inserted into BglII/NcoI sites of the pGL3-Basic vector (Promega) to generate pGL3-mp21/5 (8.8 kb). p1339 (GenBank accession number AF335419) was used to assemble the targeting vector (a gift from the Siteman Cancer Center at Washington University). p1399 contains a *loxP*-flanked *PGK-Neo* cassette (phosphoglycerate kinase promoter driving expression of neomycin phosphotransferase). The 1.8-kb EcoRI/EcoRI 3′ arm was cloned into EcoRV-digested p1339 to generate p1339-mp21/3. The 5.9-kb MluI/BamHI fragment from pGL3-mp21/5 was then cloned into KpnI-digested p1339-mp21/3 to generate the final targeting vector (mp21-pGL3).

Generation of reporter mice. RW4 embryonic stem (ES) cells (Siteman Cancer Center at Washington University) were electroporated with NotI-linearized targeting vector and selected with Geneticin (G418; Invitrogen) using established protocols (Siteman Cancer Center Murine Embryonic Stem Cell Core). A total of 144 G418-resistant ES cell colonies were analyzed for homologous recombination. Genomic DNA was digested with EcoRV followed by Southern blotting using a 5′ Southern probe (primers Forward, 5′-GCG ATA TCC AGA CAT TCA GAG-3′, and Reverse, 5′-GGA ATC CCT AGA AAC ATT GGC-3′). ES cell clone 70 was selected, and homologous recombination was confirmed for the 3′ arm by PCR using two primers (5′-TCT TGT GTT TCA GCC ACA GGC-3′ and 5′-CAA TGC AGG GGG TTG CCA CT-3′). ES cell clone 70 was determined to have a normal karyotype and was expanded and electroporated with a plasmid carrying Turbo-Cre recombinase under the control of the chicken β-actin promoter to remove the *PGK-Neo* cassette. A total of 51 ES cell clones were analyzed for excision of the *PGK-Neo* cassette. Genomic DNA was digested with EcoRV followed by Southern blotting with the 5′ Southern probe and PCR using the same primers as described above for the 3′ arm to identify clones lacking the *Neo* cassette. ES cell clone 70-58 was selected and found to have a normal karyotype. This clone was microinjected into C57BL/6 blastocysts, which were subsequently implanted into the uteri of pseudopregnant C57BL/6 × C3H foster mothers. Male chimeras selected based on the percentage of agouti color were mated to C57BL/6 females. Germ line transmission was determined by agouti coat color. F1 animals were tested for the targeted *p21* allele by PCR analysis of tail DNA. PCR analysis of tail DNA was performed with three primers (a, 5′-TCT TGT GTT TCA GCC ACA GGC-3′; b, 5′-CTG TCA GGC TGG TCT GCC TCC-3′; c, 5′ CGA ACG GAC ATT TCG AAG TAC-3′). The sizes of the wild-type (WT) and recombinant alleles were 453 bp and 208 bp, respectively. The *Trp53*$^{+/-}$ mouse line was obtained from Jackson Labs (catalog number 000058). All mice were crossed to 129X1/SvJ and B6(Cg)-Tyr^{c-2J}/J mice to obtain a white coat color for imaging.

Generation and culturing of MEFs. MEFs were generated as described previously (12), cultured in a 5% O_2 incubator, and frozen at passage 2. MEFs were cultured in complete MEF medium consisting of Dulbecco's modified Eagle's medium (DMEM; high glucose with L-glutamine; Gibco,) supplemented with 10% fetal bovine serum (FBS), 100 U/ml penicillin, 100 U/ml streptomycin (Gibco), 2 mM L-glutamine (Gibco), 100 μM nonessential amino acids (Gibco), and 140 μM 2-mercaptoethanol (Bio-Rad). Imaging experiments were performed in black-walled 24-well plates (Midwest Scientific, St. Louis, MO) in medium lacking phenol red and containing 0.5 mM D-luciferin (Biosynth). All experiments were conducted with early-passage cells (P2 to P5), and at least three different lines were used for each genotype. Cells were irradiated in a ^{60}Co source. Serum starvation experiments were performed with cells plated at subconfluency. A total of 0.2×10^4 to 0.7×10^4 cells were seeded in 24-well black-walled tissue culture dishes for BLI and 0.5×10^5 to 2×10^5 cells were seeded in 10-cm tissue culture dishes for Western blotting. One day after plating, cells were washed twice with low-serum MEF medium (0.1% FBS) and cultured in low-serum medium for 48 h. Cells were then incubated in low-serum medium with the indicated concentrations of U0126 (Promega) in dimethyl sulfoxide (DMSO; Sigma) or DMSO alone for 30 min, followed by incubation in MEF medium containing 10% FBS and supplemented with the indicated concentrations of U0126 or vehicle (DMSO). Bioluminescence imaging was performed using an IVIS Lumina or IVIS 50 apparatus (Caliper) with identical instrument, field-of-view, f-stop, exposure, and binning settings within an experiment (16).

shRNA. For shRNA knockdown, lentiviruses were produced using pLKO.1 plasmids that contained shRNA sequences and were cotransfected with packaging plasmids as described previously (36). shRNA sequences were tested for p53 knockdown (pLKO.1 shTrp53, CCG ACC TAT CCT TAC CAT CAT; RNAi Consortium) and compared to a scrambled control (pLKO.1 Scr, CCTAA GGTTA AGTCG CCCTC GCTCT AGCGA GGGCG ACTTA ACCTT AGG; Addgene) (31). All cells were selected in puromycin (2 μg/ml; Invitrogen).

Real-time PCR. RNA was isolated from MEFs by using the RNeasy kit (Qiagen). RNA was reverse transcribed with random primers (SuperScript II; Invitrogen). Standard curves were generated using cDNA from *p53*$^{+/+}$ and *p53*$^{-/-}$ MEFs of each sample within an experiment. The standard curve for each primer was generated from the logarithmic equation fitting the cycle thresholds for 400, 200, 100, 25, 12.5, and 1 ng, and all R^2 values were greater than 0.99. The standard curve was run on each plate at least in duplicate. Each sample was tested in triplicate at 50 ng cDNA, except in the *p53*$^{-/-}$ samples, where *p21* and *FLuc* levels at 50 ng were outside the linear range of the standard curve, and so these samples were run in triplicate undiluted from the cDNA reaction mixture. Real-time PCR was performed with SYBR green master mix (Agilent) and a 100 nM concentration of the specific primer set, in a Bio-Rad CFX96 PCR instrument (95°C for 10 min, then 40 cycles of 95°C for 30 s, 61°C for 1 min, and 74°C for 1 min). Primers were the following: *p21* forward, 5′-GAC AAG AGG CCC AGT ACT TCC T-3′; *p21* reverse, 5′-CAA TCT GCG CTT GGA GTC ATA-3′; *FLuc* forward, 5′-CGT CGC CAG TCA AGT AAC AAC C-3′; *FLuc* reverse,

5′-CAC GGC GAT CTT TCC GCC-3′; 18S forward, 5′-CAT TCG AAC GTC TGC CCT ATC-3′; 18S reverse, 5′-CCT GCT GCC TTC CTT GGA-3′.

For whole-tissue RNA extraction, mice were perfused with diethyl pyrocarbonate-treated phosphate-buffered saline (PBS) followed by a 3-min perfusion with RNALater (Ambion). Organs were then dissected and flash-frozen in RNALater. RNA was isolated from homogenized whole tissues by using TRIzol (Invitrogen). Quality of whole-tissue RNA was determined by gel electrophoresis or spectrophotometry, and only intact samples were analyzed. RNA was reverse transcribed with random primers (SuperScript II; Invitrogen). cDNA was pooled from whole-tissue lysates to generate a standard curve. All samples were run in triplicate with 50 ng cDNA. Real-time PCR was performed as described above.

RNA was isolated from laser capture microdissected tissue using the RNeasy microkit (Qiagen). RNA was reverse transcribed using the High-Capacity cDNA reverse transcription kit (Applied Biosystems). Real-time PCR was performed using TaqMan primers and probes for *p21* (Mm00432448_m1) and *actin* (4352341E; Applied Biosystems). Due to the small volume of RNA isolated from laser capture microdissection, a standard curve could not be generated, and the ΔC_T method was used for analysis. Relative expression levels of *p21* and *FLuc* were calculated by normalizing to *actin* or 18S levels (see Fig. 2, 4C, and 7B) and then to mock-irradiated samples within each genotype (see Fig. 4F), to *p21* mRNA (see Fig. 7C), or to wild-type control levels (see Fig. 12).

Western blotting. Cells were lysed in mammalian cell lysis buffer (MCLB; 50 mM Tris-HCl [pH 8.0], 2 mM dithiothreitol, 5 mM EDTA, 0.5% NP-40, 100 mM NaCl, 1 mM microcystin [Sigma Chemical Co.], 1 mM sodium orthovanadate, 2 mM phenylmethylsulfonyl fluoride) supplemented with protease (Sigma Chemical Co.) and phosphatase inhibitor (Calbiochem) cocktails. Clarified lysates were resolved by SDS-PAGE (10%/15% layered SDS gel) and transferred to nitrocellulose membranes for Western blotting. Membranes were blocked in TBST (20 mM Tris-HCl [pH 7.6], 137 mM NaCl, 0.1% Tween 20) containing 5% nonfat milk and incubated overnight in primary antibody diluted in either TBST–1% nonfat milk or TBST–5% BSA containing 0.05% sodium azide. Membranes were washed in TBST, incubated with fluorescent- or horseradish peroxidase (HRP)-conjugated secondary antibody for 1 h in TBST–1% nonfat milk, and washed again in TBST. Blots were analyzed using the Odyssey imaging system (LI-COR Biosciences) or incubated with the enhanced chemiluminescence system (Pierce) and exposed to film. Quantification was performed in ImageJ (2). Primary antibodies included anti-p21 at 1:1,000 (F5; Santa Cruz Biotechnology), anti-FLuc at 1:10,000 (sc6246; Santa Cruz Biotechnology), anti-actin at 1:10,000 (A4700; Sigma Chemical Co.), anti-p53 at 1:1,000 (1C12; Cell Signaling), antitubulin at 1:1,000 (YL1/2; AbCam/2), anti-cyclophillin A at 1:1,000 (2175; Cell Signaling), anti-phospho-p44/42 Erk1/2 at 1:1,000 (D13.14.4E; Cell Signaling), and anti-p44/42 Erk1/2 at 1:2,000 (L34F12; Cell Signaling). Secondary antibodies for the Odyssey system were from LI-COR Biosciences and included donkey anti-rabbit IRDye-800CW, donkey anti-mouse IRDye-800CW, and donkey anti-mouse IRDye680CW. Secondary antibodies for autoradiography were peroxidase conjugated, AffiniPure goat anti-mouse (Jackson), HRP–rabbit anti-rat (Zymed), and HRP–goat anti-rabbit (Invitrogen).

Immunohistochemistry. Mouse tissues were fixed in Bouin's solution (Sigma Chemical Co.) overnight, progressively dehydrated through gradients of ethanol, and then paraffin embedded. Tissues were sectioned at a thickness of 5 μm. Trilogy (Cell Marque) was used for deparaffinization, rehydration, and antigen retrieval. Vaginal sections were blocked using Rodent Block M (Biocare) and then incubated with anti-FLuc antibody (sc6246; Santa Cruz Biotechnology) diluted 1:1,000 in PBS containing 3% nonfat milk and 0.1% Triton X-100 at 4°C overnight. Sections were washed and then incubated with secondary antibody Alexa-Fluor 594 goat anti-rabbit (Invitrogen) at room temperature for 1 h. Secondary antibody was diluted 1:1,000 in fluorescent diluent (Biocare) with XR factor (1:300; Biocare). Images were acquired on an Olympus BX61 microscope with a Hamamatsu ORCA R^2 monochrome camera and the Microsuite Biological Suite software. Images were processed equally for signal intensity and color merge by using ImageJ (2). Penis sections were prepared and incubated with anti-FLuc antibody as described above, with an additional blocking step of 3% H_2O_2 in methanol for 30 min to block endogenous peroxidase activity immediately following antigen retrieval. Tissue sections were washed in PBS and incubated with secondary anti-rabbit antibody–HRP (no dilution; Dako) at room temperature for 1 h. Slides were washed in PBS, incubated in freshly made diaminobenzidine substrate (Invitrogen) for 5 min, rinsed in distilled water followed by PBS, and counterstained with hematoxylin (Invitrogen). Images were acquired with an Olympus BX51 microscope with an Olympus DP71 color camera using the Olympus Controller software.

Bioluminescence imaging of mice and organs. Reporter mice were implanted with microosmotic pumps (Alzet 1007D; 0.5 μl/h for 7 days) containing 100 μl of 50-mg/ml D-luciferin (Biosynth) as described previously (15). Pumps were implanted at least 16 h before the start of the experiment to allow for equilibration of D-luciferin and mouse recovery. For irradiation experiments, mice were placed in a chamber, transported to a ^{137}Cs source irradiator, and exposed to the indicated dose of IR or remained outside the irradiator chamber (mock group). Imaging was performed using an IVIS Lumina device (Caliper), and mice were anesthetized with 1.5% isoflurane through an O_2 flow modulator. Mice were anesthetized for 10 min in a holding tank and allowed to equilibrate in the IVIS for 15 min, and then the image was acquired (60 s; binning, 4). Photon flux was measured at baseline by drawing a rectangular region of interest (ROI) from the forepaws to slightly above the genitals for each mouse. The ROI was duplicated each time the mouse was imaged. The genitals and bladder were eliminated from the ROI because of the large variation in signal generated from this region of the mouse by excretion of D-luciferin. Data were expressed as total photon flux (photons/s) or normalized as fold increases, expressed as posttreatment/pretreatment and/or posttreatment/vehicle image ratios. For *ex vivo* experiments, a predissection image was taken as described above. Mice were then sacrificed and organs were rapidly removed, weighed, placed in individual wells of a 24-well black-wall plate, and imaged within 25 min of sacrifice (30-s exposure; binning, 4). Corresponding gray-scale photographs and color luciferase images were superimposed and analyzed with LivingImage 3.2 (Caliper) and Igor (Wavemetrics) image analysis software.

Low-light microscopy. Male and female $p21^{+/FLuc}$ mice were sacrificed and organs isolated (small intestine, liver, and penis or vagina). Organs were placed in ice cold Hanks buffered saline solution (HBSS; pH 7.4; Sigma Chemical Co.). Livers were sectioned into 200-μm sections on a vibratome (immersed in HBSS maintained at 4°C), and the small intestine and vagina were cut into 200-μm sections using a tissue chopper. Penises were cut longitudinally to create a flat surface, and then sections were cut using two attached razor blades with a 300-μm spacer between them. Organ sections were placed on an organotypic Millicell culture insert (Millipore) in a 35-mm petri dish containing HEPES-buffered DMEM supplemented with B27 (Invitrogen), 0.1 mM D-luciferin (BioThema), and 100 U/ml penicillin, 100 U/ml streptomycin (Gibco). Small intestines were incubated in crypt culture medium composed of Advanced DMEM/F-12 (Gibco), 50 ng/ml EGF (Peprotech Inc.), 100 ng/ml Noggin (Peprotech Inc.), 500 ng/ml R-spondin (R&D Systems) containing 10 μM D-luciferin (BioThema) (32). All images were completed within 3 h of organ isolation. Penises and vaginas were incubated in 1 nM SYTO 11 green fluorescent nucleic acid stain (Invitrogen). To orient vaginal tissue, the lumen was stained with SYPRO ruby (Invitrogen), a protein-binding fluorescent dye. All images were obtained with a Versarray back-thinned illuminated charge-coupled-device (CCD) camera (Princeton Instruments) or an iXon DU-897E EM CCD camera (Andor Technology). Cameras were coupled to a TE-2000 Nikon inverted microscopes equipped with custom light-tight environmental chambers (InVivo Scientific) that prevented light leaks and kept a constant temperature of 37°C. Image acquisition was controlled with Winview32 and Micro-Manager (www.Micro-Manager.org) software packages. Image processing was performed with ImageJ software (2) and included subtraction of a background image, removal of random bright spots (using the despeckle filtering algorirthm in ImageJ), and adjusting the brightness and contrast equally across the entire image. Intensity-scale ramps were scaled and normalized to the time over which the image was acquired and are represented as relative light units (RLU)/min. Pseudocolored images were generated using the RainbowRGB look-up table (LUT) on the bioluminescence image, which was then merged to the bright-field image.

Isolation and culturing of primary hepatocytes from reporter mice. Primary hepatocytes were isolated from $p21^{+/FLuc}$ mice by hepatic portal collagenase perfusion as described previously (19, 20). Briefly, the liver was perfused with collagenase (Sigma Chemical Co.), the liver sheath was disrupted, and cells were passed through a 70-μm filter. Cells were washed twice with DMEM, and double-nucleated hepatocytes were pelleted at 65 × *g* and plated in collagen-1-coated 6-well plates (BD Biosciences) in DMEM (Invitrogen) supplemented with 10% fetal bovine serum (non-heat inactivated), 100 U/ml penicillin, 100 U/ml streptomycin (Gibco). The next day, the medium was changed to hepatocyte imaging medium (same as above except with phenol red-free DMEM [Gibco] and 0.5 mM D-luciferin [Biosynth]). Cells were allowed to equilibrate for 1 h, and bioluminescence was measured using the IVIS Lumina (Caliper) as described above for MEFs.

Laser capture microdissection. Tissues were dissected from $p21^{+/+}$ or $p21^{FLuc/FLuc}$ mice, immediately frozen in optimal cutting temperature (OCT) compound (TissueTek), and stored at −80°C. Sections of 15 to 20 μm were cut on a cryostat and were placed on PEN membrane slides (Leica). Unstained slides were stored in a desiccator at −80°C. Tissues were fixed in 70% ethanol (20 s) and rehydrated in RNase-free water (10 times). Nuclei were stained with methyl green (10 times; Vector), rinsed in RNase-free water, counterstained with

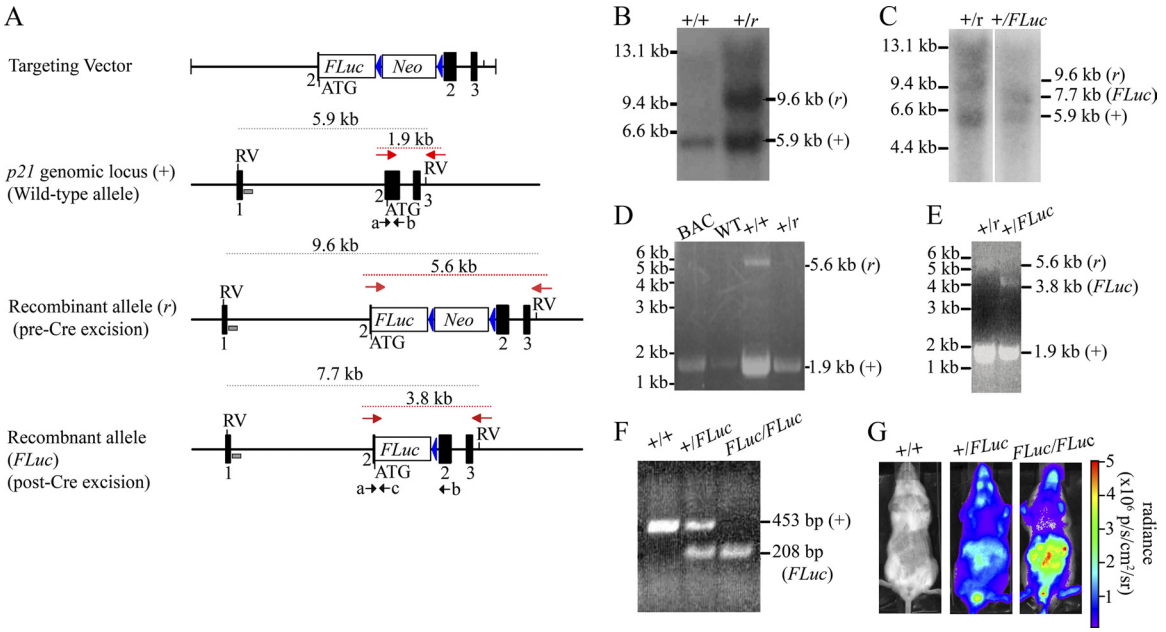

FIG. 1. Generation of *p21-FLuc* reporter mice. (A) Structure of the targeting vector, wild-type *p21* genomic allele (+), and recombinant allele before (r) and after (FLuc) Cre-mediated excision. The coding region of the mouse *p21* gene was disrupted by insertion of codon-optimized firefly luciferase cDNA (*FLuc*) containing simian virus 40 poly(A) sequences and a neomycin phosphotransferase cDNA cassette (*Neo*) driven by the phosphoglycerine kinase promoter as a selectable marker. Upon homologous recombination, the *FLuc* cDNA utilizes the ATG start codon of endogenous *p21* in exon 2. The orientation of *Neo* cassette coding sequences was opposite to that of *FLuc*. Exons are represented by black boxes; EcoRV sites are denoted by RV; *loxP* sites as shown as blue triangles; the 5′ Southern probe is indicated by a gray box; 3′ PCR primers are indicated by the red arrows, and genotyping primers are shown as black arrows and in lowercase letters. Sizes of expected Southern blotting and PCR products are indicated. (B) Genomic DNA from ES cell clone 70 was digested with EcoRV. Southern blotting was performed using the 5′ probe represented by the gray box in panel A. The wild-type allele (+) gave rise to a 5.9-kb digestion product, and the recombined allele (*r*) gave rise to a 9.6-kb digestion product. (C) Genomic DNA from ES cell clone 70-58 was digested with EcoRV. Southern blotting was performed using the 5′ probe represented by the gray box in panel A. The wild-type allele (+) gave rise to a 5.9-kb digestion product, the recombined allele (*r*) with the *Neo* cassette still present gave rise to a 9.6-kb digestion product, and the recombined allele with the *Neo* cassette removed gave rise to a 7.7-kb product. Size markers are indicated on the left, and product sizes are on the right. (D) Genomic DNA isolated from either a BAC clone containing *p21*, tail DNA from a wild-type mouse (WT), or two ES cell clones was amplified using PCR primers (represented by red arrows in panel A). The wild-type allele (+) gave rise to a 1.9-kb product, and the recombined allele (-) gave rise to a 5.6-kb product. (E) Genomic DNA isolated from ES cell clone 70 (+/*r*) and 70-58 (+/*FLuc*) was amplified using the PCR primers represented by red arrows in panel A. The wild-type allele (+) gave rise to a 1.9-kb product, the recombined allele (-) with the *Neo* cassette still present gave rise to a 5.6-kb product, and the recombined allele with the *Neo* cassette removed gave rise to a 3.8-kb product. Size markers are indicated on the left, and product sizes are shown on the right. (F) PCR analysis of tail DNA from wild-type (+/+), heterozygous (HT; +/*FLuc*), or homozygous (KI; *FLuc/FLuc*) knock-in mice amplified with primers indicated by the black arrows (a, b, and c) in panel A. The WT (+) allele produced a 453-bp product with primers a and b, and the recombinant (*FLuc*) allele produced a 208-bp product from primers a and c. (G) WT, HT, or KI mice were shaved and implanted with D-luciferin microosmotic pumps and imaged using the IVIS Lumina system (Caliper). Representative images of mice at baseline are shown. Photon flux is indicated in the pseudocolored heat map.

EosinY (2 times), and dehydrated in ethanol (70%, 95%, 95%, 100%, and 100%) for 1 min each. Slides were rinsed in xylene and dried in a desiccator for at least 5 min immediately prior to laser capture microdissection. Tissue sections were dissected using the Leica LMD7000 laser capture microdissection system.

Statistics. All statistics were performed using Graphpad Prism software or SPSS software. Specific statistical tests performed are noted with the data. All error bars are the standard errors of the means (SEM).

RESULTS

Generation of *p21* reporter mice. Knock-in mice expressing firefly (*Photinus pyralis*) luciferase from the endogenous *p21* promoter were generated to monitor the spatial and temporal regulation of *p21* (*Cdkn1a*) gene expression *in vitro* and *in vivo* by BLI (Fig. 1A). Homologous recombination in ES cell clones was confirmed by Southern blotting (Fig. 1B and C) and PCR analysis (Fig. 1D and E), while genotyping of offspring was performed by PCR analysis of mouse tail DNA (Fig. 1F). Whole-body bioluminescence was detected in both heterozygous (+/*FLuc*) and homozygous (*FLuc/FLuc*) knock-in mice but not wild-type (+/+) mice (Fig. 1G).

Characterization of *p21* promoter activity in reporter-derived MEFs. MEFs were generated as a way to determine if *FLuc* expression accurately reflected endogenous *p21* expression. Bioluminescence of MEFs derived from wild-type ($p21^{+/+}$) mice was within background levels as expected, while bioluminescence of MEFs derived from heterozygous knock-in animals ($p21^{+/FLuc}$) was 307-fold over the background. Bioluminescence of MEFs derived from homozygous knock-in animals ($p21^{FLuc/FLuc}$) was 2.2-fold higher than MEFs derived from heterozygous ($p21^{+/FLuc}$) littermates (Fig. 2A and B). $p21^{+/+}$ MEFs contained ~1.5-fold more *p21* mRNA than did $p21^{+/FLuc}$ MEFs (Fig. 2C). Correspondingly, *FLuc* mRNA was absent in $p21^{+/+}$ MEFs and present at ~1.8-fold-higher levels in $p21^{FLuc/FLuc}$ MEFs than in $p21^{+/FLuc}$ MEFs (Fig. 2C). Western blotting revealed an approximate 50% decrease in p21

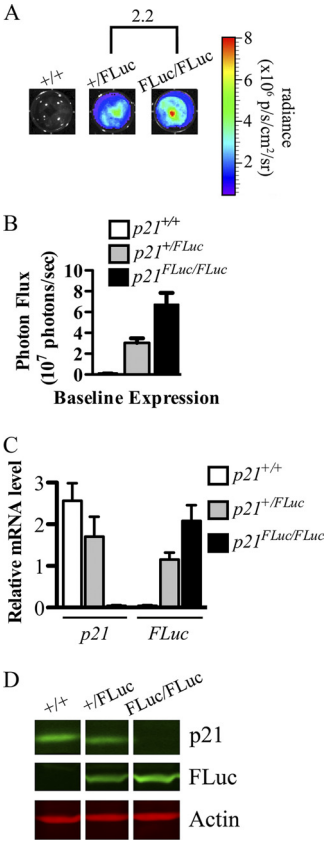

FIG. 2. *p21* promoter activity in reporter MEFs. (A and B) MEFs of the indicated genotypes were plated at equal densities in quadruplicate, and bioluminescence activity was determined. Representative wells are depicted by a pseudocolored heat map (A), and photon flux was plotted (B). (C) Relative levels of *p21* and *FLuc* mRNAs were determined by quantitative reverse transcription-PCR in MEF lines, and values were normalized to 18S rRNA. (D) Western blotting was performed to determine relative levels of p21 and FLuc in each MEF line, and actin was used as a loading control.

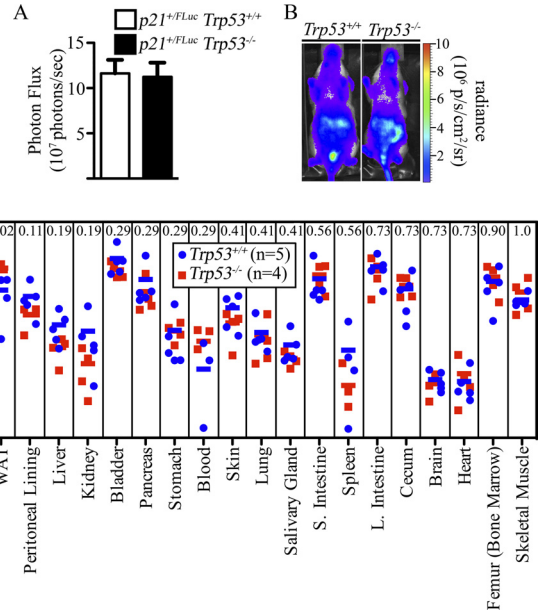

FIG. 3. *p21* expression in wild-type and *Tpr53*-null mice. $p21^{+/FLuc}$ $Trp53^{+/+}$ ($n = 14$) and $p21^{+/FLuc}$ $Trp53^{-/-}$ ($n = 9$) mice were implanted with D-luciferin microosmotic pumps, and whole-body images were obtained. (A and B) Compiled results were plotted (A), and representative mice are also shown (B). (C) Mice were sacrificed, and individual organs were isolated, weighed, and then imaged *ex vivo*. Bioluminescence of each organ is represented as the photon flux/sample weight (photons/s/g). Individual mice (squares and circles) and the group average (bars) are shown. The Mann-Whitney U Test *P* values are indicated at the top of each column.

protein in $p21^{+/FLuc}$ MEFs relative to WT MEFs, and FLuc protein levels were ~2-fold higher in $p21^{FLuc/FLuc}$ MEFs relative to $p21^{+/FLuc}$ MEFs (Fig. 2D). Overall bioluminescence, mRNA, and protein levels correlated with the *p21 WT* allele copy number (Table 1). These results indicate that reporter activity accurately reflects basal *p21* promoter expression.

Characterization of *p21* promoter activity in reporter MEFs lacking p53. To monitor *p21* promoter activity in both the presence and absence of p53, reporter mice along with their wild-type littermates were crossed to $Trp53^{+/-}$ mice, followed by intercrossing to obtain $p21^{+/FLuc}$ reporter mice with littermates wild type or null for *Trp53*. Compared to $p21^{+/FLuc}$ littermates (p53 wild type), no difference in baseline promoter activity was observed with whole-body BLI (Fig. 3A and B) or in isolated organs of p53-null $p21^{+/FLuc}$ reporter mice, with the exception of white adipose tissue (WAT), where enhanced bioluminescence was measured in p53-null WAT relative to p53 WT WAT ($P = 0.016$) (Fig. 3C). Early-passage heterozygous reporter MEFs were also generated and subjected to BLI. In contrast to live mice, basal bioluminescence measured in $p21^{+/FLuc}$ MEFs lacking p53 was ~20% of that measured in reporter MEFs with wild-type p53 (Fig. 4A, panels 1 and 3, and B). mRNAs encoding *p21* and *FLuc* were significantly reduced in p53-null heterozyous reporter MEFs relative to their p53 wild-type counterparts (9% and 10% of WT, respectively) (Fig. 4C). Similarly, both p21 and FLuc proteins were also reduced in the absence of p53 (Fig. 4D, lanes 1 and 3).

Next, MEFs were imaged to obtain baseline values and then either mock irradiated or exposed to 2.5 Gy of irradiation. Cells were then reimaged at various time points after irradiation. Representative bioluminescence images are shown in Fig. 4A, and data obtained at 4 and 12 h postirradiation are displayed graphically (Fig. 4E). Results confirmed previously published findings (11) demonstrating that IR activates the *p21* promoter in a p53-dependent manner, and they further validated that reporter MEFs accurately reflect endogenous *p21* promoter activity in response to IR. Protein (Fig. 4D) as well as mRNAs encoding p21 and FLuc (Fig. 4F) accumulated

TABLE 1. Pearson coefficients for baseline bioluminescence, mRNA, and protein levels within $p21^{+/+}$, $p21^{+/FLuc}$, and $p21^{FLuc/FLuc}$ MEFs

Assay	*r* value	*P* value
Bioluminescence	−0.70	0.005
p21 mRNA	0.88	0.002
FLuc mRNA	−0.74	0.090
p21 protein	0.97	<0.001
FLuc protein	−0.99	<0.001

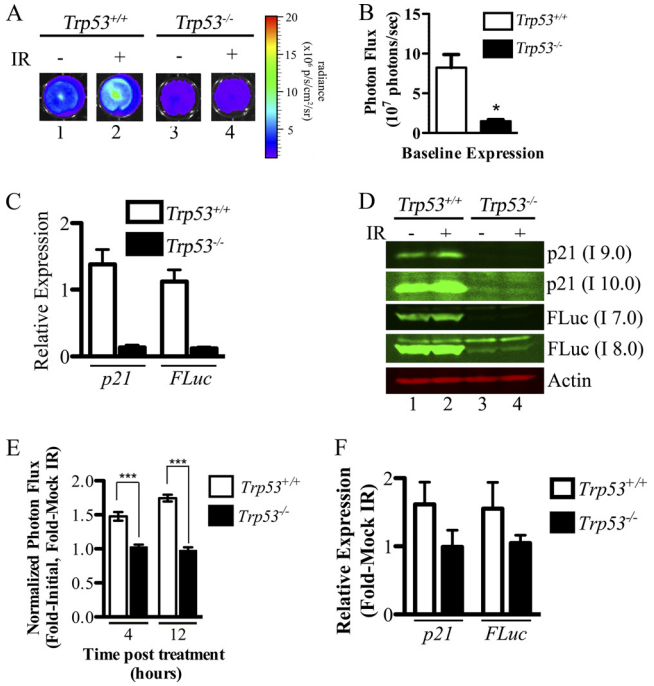

FIG. 4. IR activates the *p21* promoter in a p53-dependent manner *in vitro*. All experiments were performed with $p21^{+/FLuc}$ MEFs with the indicated p53 status. MEFs were plated at equal densities, and bioluminescence was measured at baseline ($t = 0$) and at 4 and 12 h after mock irradiation or exposure to 2.5 Gy of IR. (A) Representative images of MEFs obtained 12 h after IR. (B) Absolute photon flux values at baseline. *, $P = 0.015$, two-tailed t test. (C to E) To plot the response to IR, data were normalized to the baseline value for each replicate and then to the mock-irradiated sample ($P < 0.001$ by 2-way analysis of variance [ANOVA], comparing $Trp53^{+/+}$ MEFs to $Trp53^{-/-}$ MEFs. ***, $P < 0.001$ by Bonferroni posttest of 2-way ANOVA results. Additionally, MEFs were mock irradiated or exposed to 2.5-Gy IR, and 12 h later mRNA was isolated. Levels of *p21* and *FLuc* mRNA 12 h post-IR relative to a standard curve and 18S rRNA (C) as well as normalized to mock-irradiated samples within each genotype (F) are shown. MEFs were mock irradiated or exposed to 5-Gy IR and harvested 4 h later, and Western blotting was performed for the indicated proteins (D). Different exposures using the Odyssey imaging system are shown. A higher intensity (I) is equivalent to a longer exposure time. For experiments involving BLI and relative mRNA determinations, 3 separate MEF lines were used per genotype, and each line was plated in at least triplicate per treatment.

concordantly in irradiated reporter MEFs in a p53-dependent manner.

Regulation of *p21* expression during cell cycle reentry from quiescence. Next, the contribution made by p53 to the ability of MEFs to reenter the cell cycle from quiescence was examined. $p21^{+/FLuc}$ reporter MEFs that were either wild type or null for p53 were cultured in 0.1% serum for 48 h in order to induce growth arrest (Fig. 5A). As seen in Fig. 5B, there was a significant decrease in bioluminescence over the 48-h period, and the observed loss of *p21* expression was independent of p53 status. Interestingly, *p21* expression was induced when p53-null but not p53 wild-type MEFs were cultured in 10% FBS to stimulate cell cycle reentry (Fig. 5B). The ERK/MAPK pathway has been shown to activate *p21* expression in response to serum stimulation (6, 25). Therefore, we tested whether inhibition of MEK (with the kinase inhibitor U0126) blocked induction of *p21* expression by serum restimulation. Cells that had been cultured in 0.1% FBS for 47.5 h were treated with either vehicle (DMSO) or a range of U0126 concentrations for 30 min. After the 30-min preincubation period, cells were cultured in medium containing 10% FBS together with either DMSO or U0126, and BLI was performed at the indicated time points. Photon flux was normalized to baseline values obtained from cells cultured in 0.1% FBS for 48 h ($t = 0$ in Fig. 5A). Note that an approximate 6-fold induction of bioluminescence was measured in p53-null cells within 5 h of culturing in 10% FBS (Fig. 5C), and a dose-dependent inhibition of *p21* expression by U0126 was observed under these conditions (Fig. 5C and D). This suggests that in the absence of p53, serum stimulation acts through the ERK/MAPK pathway to activate *p21* expression. As is shown in Fig. 5B, serum stimulation was ineffective at inducing *p21* expression in p53 wild-type MEFs (Fig. 5E), and in p53 wild-type MEFs, inhibition of *p21* expression was only observed at the very highest doses of U0126 (30 and 100 μM), where off-target effects of the drug are expected (Fig. 5E and F). Western blotting revealed that p21 protein levels were also elevated when p53-null but not wild-type MEFs were stimulated with serum, and the ability of serum to increase p21 was blocked by U0126 (Fig. 5G). Note that 10% FBS stimulated ERK phosphorylation, and this was blocked with 10 μM U0126 in both p53 wild-type and null MEFs (Fig. 5H). Taken together these findings suggest that p53 blocks quiescent MEFs from activating *p21* expression in response to serum stimulation. Given that ERK phosphorylation is induced normally under these conditions, the block in signaling must be at a point downstream of ERK/MAPK activation (Fig. 6E).

If p53 prevents the ERK/MAPK pathway from activating *p21* expression in serum-stimulated quiescent cells, then knockdown of p53 should result in activation of the *p21* promoter and increased levels of p21 protein in p53 wild-type MEFs under these conditions. As seen in Fig. 6A, efficient knockdown of p53 was achieved in p53 wild-type MEFs upon lentiviral infection. Importantly, when p53 was knocked down, p21 levels rose following serum stimulation (Fig. 6B, lanes 5 and 6, and C), and this response was inhibited by U0126 (Fig. 6B, lanes 6 and 8, and C). Bioluminescence followed similar trends, in that knockdown of p53 now sensitized *p21* expression to U0126 (Fig. 6D). As expected, p21 levels did not rise when quiescent p53 wild-type MEFs expressing scrambled shRNAs were cultured in 10% FBS (Fig. 6B, lanes 1 and 2, and C), and U0126 treatment did not decrease overall levels of p21 in these cells (Fig. 6B, lanes 2 and 4, and C).

Analysis of *p21* promoter activity in individual organs of reporter mice. Individual organs were freshly isolated from reporter mice to determine the localization and intensity of basal *p21* promoter activity *in vivo* (Fig. 7 and 8). To account for size differences between various organs within a single mouse as well as the same organ in different mice, organ photon flux was normalized to organ weight. As seen in Fig. 7, values measured in individual organs ranged from 1×10^6 to 1×10^9 photons/s/g. Bioluminescence was detected in every organ that was examined; even the low signals measured in blood, heart, brain, and spleen were above background levels. These results suggested that the *p21* promoter was ubiquitously active in unperturbed mice. Within the quantitative limits in-

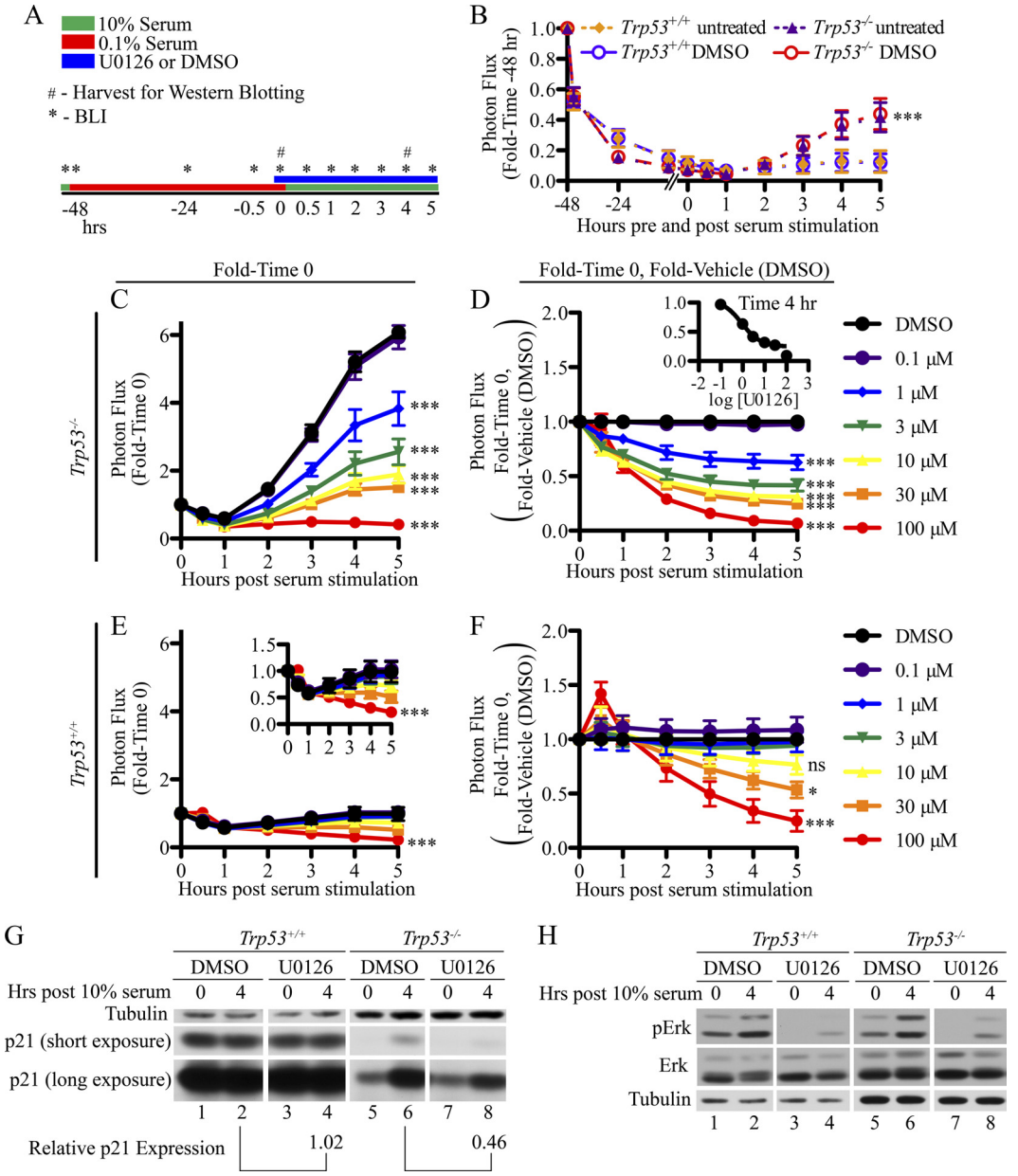

FIG. 5. Regulation of *p21* expression during cell cycle reentry from quiescence. (A) Overall experimental strategy yielding the results shown in panels B to H. Cells were plated at subconfluency and the following day incubated in medium containing 0.1% FBS for 47.5 h. Cells were then cultured in medium (0.1% FBS) in the absence or presence of DMSO for 30 min, followed by culturing in medium containing 10% FBS in the presence or absence of DMSO. (B) BLI was performed at the indicated time points. Photon flux measured at each time point was normalized to photon flux measured prior to serum starvation. A Bonferroni posttest of a 2-way ANOVA showed significance between the $Trp53^{+/+}$ and $Trp53^{-/-}$ response. Differences were not observed between DMSO and untreated cells within a given genotype.***, $P < 0.001$. Cells were plated at subconfluency and the following day incubated in medium containing 0.1% FBS for 47.5 h. (C to H) Cells were then cultured in medium (0.1% FBS) containing DMSO or the indicated concentrations of U0126 for 30 min, followed by culturing in medium containing 10% FBS together with either DMSO or U0126. BLI (C to F) and Western blotting (G and H) were performed at the indicated times. Photon flux was normalized to baseline values obtained from cells cultured in 0.1% FBS for 48 h (C and D) followed by normalization to DMSO-treated samples (D and F). The inset in panel D is a dose-response curve generated from the data shown in panel D for the 4-h time points. The inset in panel E is the same data shown in panel E but expanded on a different scale. Asterisks in panels C to F represent significance as tested by Bonferroni posttest comparing U0126 doses to DMSO from a 2-way ANOVA. ***, $P < 0.001$; *, $P < 0.05$; ns, nonsignificant. Cells were harvested at the 4-h time point for Western blotting (G and H). Film exposure times in panel G were 15 s (p21 short exposure), 5 min (p21 long exposure), or 30 min (tubulin), and in panel H exposure times were 5 s (pERK), 30 s (ERK), and 30 s (tubulin). Relative *p21* expression shown in panel G was first normalized to tubulin, followed by normalization to the indicated control sample.

troduced by different optical densities of the various tissues (21), bioluminescence was greatest in the penis, bladder, vagina, intestines, femur (containing bone marrow), skin, and WAT. To confirm that *FLuc* mRNA levels accurately represented endogenous *p21* mRNA levels, RNA was isolated from livers, spleens, kidneys, and small intestines of $p21^{+/FLuc}$ mice, and *p21* and *FLuc* mRNA levels were quantitated. As seen in Fig. 7B and C, *p21* and *FLuc* mRNA levels were concordant in

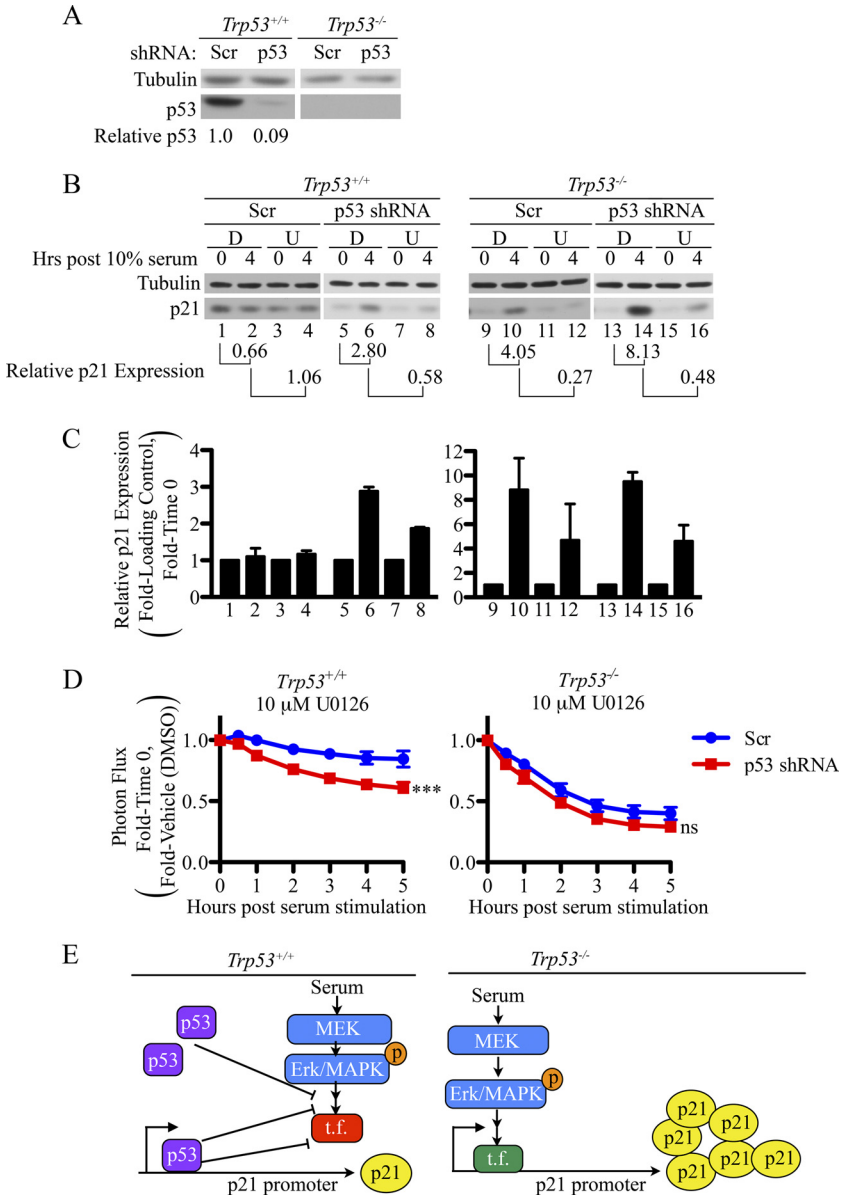

FIG. 6. p53 inhibits activation of the *p21* promoter during cell cycle reentry from quiescence. (A) MEFs infected with recombinant lentiviruses encoding either control or p53-specific shRNA were lysed and analyzed by Western blotting. The displayed data are representative of 3 independent experiments performed in three different MEF lines. (B to D) MEFs expressing control or p53-specific shRNAs were plated and treated as illustrated in Fig. 5A. Representative Western blots are shown (B), and compiled data from three separate experiments are shown graphically (C). Exposure times in panel B were 2 min (tubulin, *p21* [$Trp53^{-/-}$ samples]), and 10 s (*p21* [$Trp53^{+/+}$ samples]). BLI was performed at the indicated time points. Photon flux was normalized to baseline values obtained from cells cultured in 0.1% FBS for 48 h followed by normalization to DMSO-treated samples (D). Asterisks in panel D represent significance as tested by Bonferroni posttest comparing U0126 doses to DMSO with a 2-way ANOVA. ***, $P < 0.001$; ns, nonsignificant. (E) Model based on data shown in Fig. 5 and here. t.f., transcription factor.

all tissues with the exception of liver, where *Fluc* mRNA levels were slightly higher than *p21* mRNA levels.

Analysis of *p21* promoter activity in irradiated reporter mice. Mice were subjected to whole-body irradiation to determine if IR activates the endogenous *p21* promoter in a p53-dependent manner *in vivo*. Baseline images were obtained, and then mice were either mock irradiated or exposed to 2.5-Gy IR. Mice were then reimaged at various times posttreatment. Representative images are shown at 0 and 8 h posttreatment (Fig. 9A), and data are presented graphically in Fig. 9B. Whole-body bioluminescence of p53 wild-type reporter mice increased following IR treatment and peaked by 8 h. Bioluminescence then steadily declined until 24 h post-IR and remained stable but above baseline out to 36 h. Enhanced bioluminescence was not observed in reporter mice lacking p53 relative to mock-irradiated mice, confirming that p53 regulates the *p21* promoter in response to IR *in vivo*. Note the small, but highly reproducible, p53-independent transient increase in bioluminescence for several hours after the procedure (perhaps related to handling the mice during transport to and from the

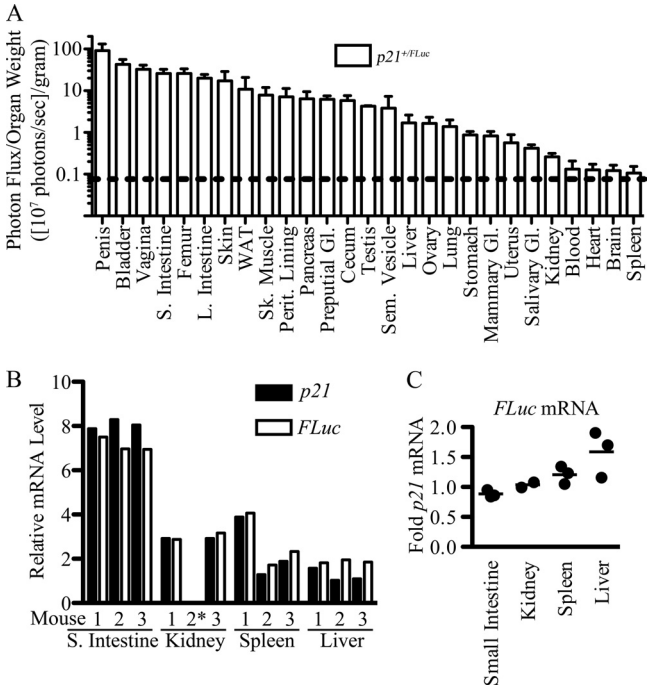

FIG. 7. Reporter expression in individual mouse organs. $p21^{+/FLuc}$ mice were implanted with D-luciferin microosmotic pumps for 1 to 3 days. Mice were sacrificed and organs were imaged *ex vivo*. To account for variation in organ size from mouse to mouse, organ weights were determined prior to BLI. (A) Bioluminescence of each organ is represented as photon flux/sample weight (photons/s/g). The graph was plotted using a logarithmic scale, and the dotted line represents the background signal detected in organs of WT mice. Relative levels of *p21* and *FLuc* mRNA were determined by quantitative reverse transcription-PCR in the indicated organs of $p21^{+/FLuc}$ mice ($n = 3$), and values were normalized to 18S rRNA (B), followed by normalization to *p21* mRNA (C). Asterisks note where the RNA isolated was not of a high enough quality for analysis.

irradiator), an apparent stress response we have observed in all groups during a variety of procedures.

Next, individual organs were isolated 8 h after treatment to determine which organs contributed to the increase in whole-body bioluminescence following IR (Fig. 9C and D). Bioluminescence was observed to increase in nearly all organs tested, but most significantly in small intestines and pancreas. Other organs that showed a significant increase were brain, large intestine, salivary gland, spleen, lung, and heart (Mann-Whitney U test) (Fig. 9C). No significant change was detected in response to IR in the peritoneal lining, liver, kidney, stomach, skin, cecum, femur containing bone marrow, or skeletal muscle (Fig. 9D). IR has previously been reported to increase p21 mRNA and protein levels in small and large intestines (7, 27, 38), brain (7, 24, 27), salivary gland (18), spleen (7, 24, 27), lung (7, 24, 27), and heart (7, 24), but the observed increase in the pancreas was a novel finding of our study.

***p21* promoter activity in specific regions of individual organs.** To localize the origin of luciferase activity within specific regions of individual organs, we employed low-light microscopy (Fig. 10). Imaging was performed using microscopes with custom-built, light-tight environmental chambers to avoid external light leaks and to control for temperature. Organs were isolated, immediately sectioned, and then placed in appropriate buffers to maintain viability. In some cases, SYTO 11 green fluorescent stain was used to visualize nucleic acid (nuclei) and SYPRO ruby was used as a protein stain. Tissue autofluorescence (Autofluor) was used to complement bright-field imaging. Bright-field (Fig. 10, column 1) and bioluminescent (Fig. 10, column 2) images were acquired for all tissues; the latter are represented as pseudocolored heat maps over the bright-field images in column 3. *p21* promoter activity was visualized throughout the villi of the small intestines and just inferior to the villi in the superior regions of crypts (Fig. 10A). This indicated that *p21* expression was turned on as cells exited their proliferative phase and began to terminally differentiate into the various epithelial cell types of the small intestine. *p21* promoter activity was widely dispersed throughout the liver, and fractionation studies confirmed luciferase activity in freshly isolated hepatocytes (Fig. 10B). *p21* promoter activity was also observed in the epithelial cell layer under the keratinized penile spines (Fig. 10C and D). The autofluorescence of the spine validated that luciferase activity originated from the base of the spine and not from within the spine itself (Fig. 10D, columns 4 and 5). Finally, *p21* promoter activity was localized to the epithelial cell layer of the vagina (Fig. 10E). The vaginal lumen was identified by bathing it in SYPRO ruby protein stain prior to dissection (column 5). SYTO 11 nucleic acid stain was used to identify the adventitia and muscularis layers of the vagina (column 4). As seen in column 6, bioluminescence was detected between these two markers, specifically, in the epithelial cell layer. Immunofluorescent staining confirmed that FLuc protein was specifically localized to the epithelial cell layer of the vagina (Fig. 11A), and immunohistochemistry confirmed that FLuc is localized in the epithelium at the base of penile spines (Fig. 11B). Finally, laser capture microdissection followed by real-time PCR confirmed that endogenous *p21* mRNA was present in the epithelial layers of the vagina and penis (Fig. 12). Taken together, we conclude that the endogenous *p21* promoter is widely active under basal conditions in organs throughout the body as well as in cell-type-specific compartments and niches of these organs not previously appreciated.

DISCUSSION

We generated and characterized knock-in *p21 luciferase* reporter mice, and this enabled noninvasive, real-time monitoring of endogenous *p21* promoter activity, both spatially and temporally, in the context of living mice and in cells derived from these mice. To validate these reporter mice, we asked whether p53 was required for basal and damage-induced expression of the *p21* promoter in mice and in MEFs. In addition, we analyzed p53-dependent and -independent regulation of *p21* expression as cells reentered the cell cycle from quiescence.

Loss of p53 had profound effects on basal expression of the *p21* promoter in cultured MEFs (Fig. 4). In contrast to live mice, there was a 5-fold reduction in baseline bioluminescence measured in early-passage MEFs obtained from p53-null mice compared with p53 wild-type mice. A decrease in *p21* promoter activity was also validated at the level of both mRNA (Fig. 4C) and protein (Fig. 4E). These findings indicated that the *p21*

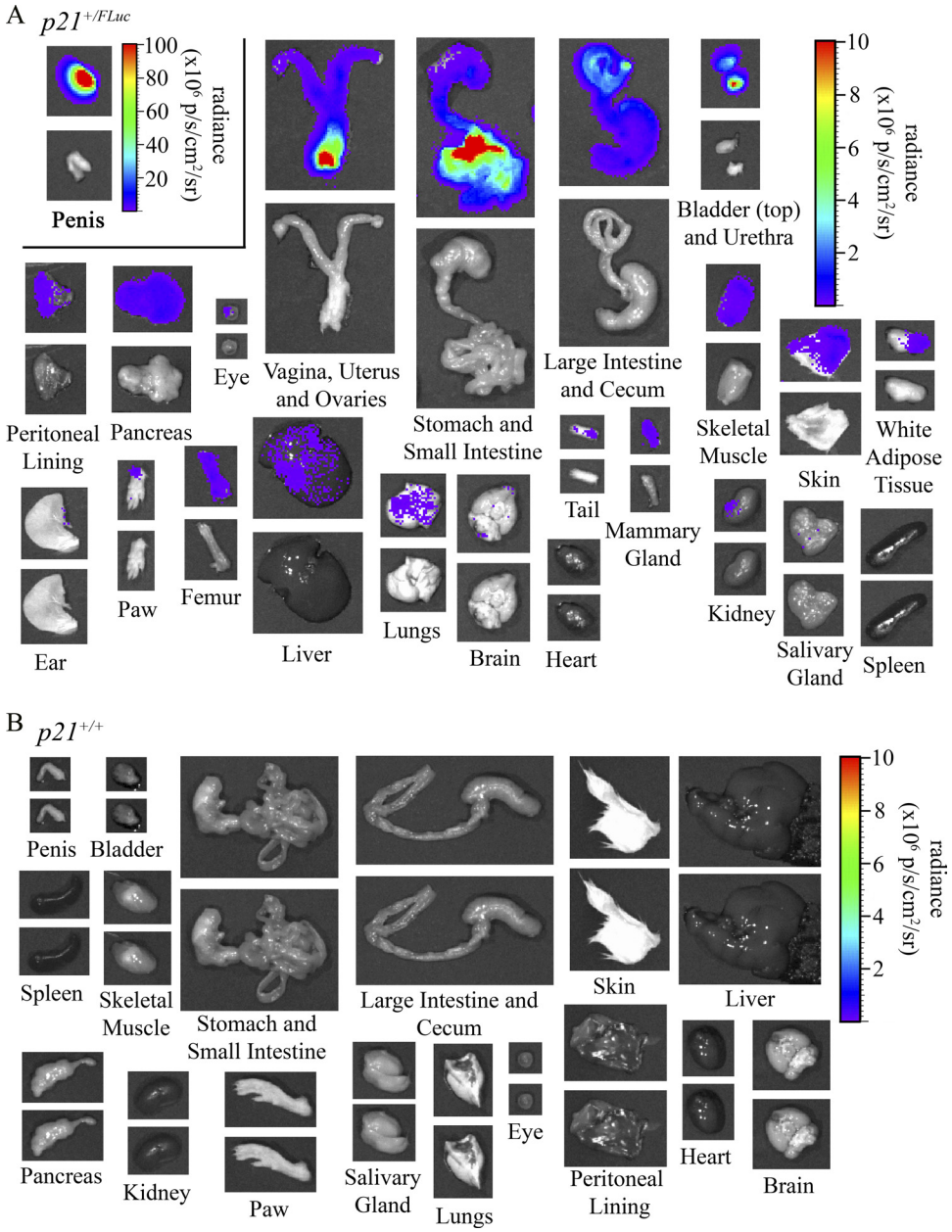

FIG. 8. Bioluminescence in individual organs of reporter and control mice. $p21^{+/FLuc}$ and $p21^{+/+}$ mice were implanted with D-luciferin microosmotic pumps. Organs were dissected, and bioluminescence was determined within 25 min of sacrifice. (A) Organs from the same female reporter mouse ($p21^{+/FLuc}$) and the penis from a male $p21^{+/FLuc}$ reporter mouse. (B) Organs isolated from a male wild-type control mouse ($p21^{+/+}$). Organ bioluminescence is represented as a pseudocolored heat map superimposed on the organ in the upper panel, and the same photograph of the organ is provided in the lower panel. Scale bars for the heat maps are provided in each panel.

promoter was activated in MEFs in a p53-dependent manner as a result of culturing cells *ex vivo*, consistent with a process that has been termed "culture shock" (33). As expected, the ability of IR to induce *p21* promoter activity in MEFs required a functional p53 pathway (Fig. 4). An increase of *p21* promoter activity was also observed in reporter mice following IR exposure, which was also p53 dependent (Fig. 9). Organ analysis *ex vivo* demonstrated that post-IR signals increased in all organs tested but most significantly in the small intestine, pancreas, and brain.

p21 expression has been shown to be activated in response to serum stimulation through the ERK/MAPK pathway. This leads to assembly of cyclin D/CDK4 complexes in order to promote cell cycle progression (6, 9, 22, 25, 27). We observed activation of *p21* expression and increases in p21 protein when quiescent MEFs were stimulated by serum, but only in *Trp53*-null cells (Fig. 5 and 6). The addition of serum to early-passage quiescent *Trp53* wild-type MEFs induced MEK activation as evidenced by increases in ERK phosphorylation, but the *p21* promoter was not activated (Fig. 6E). Thus, p53 appears to

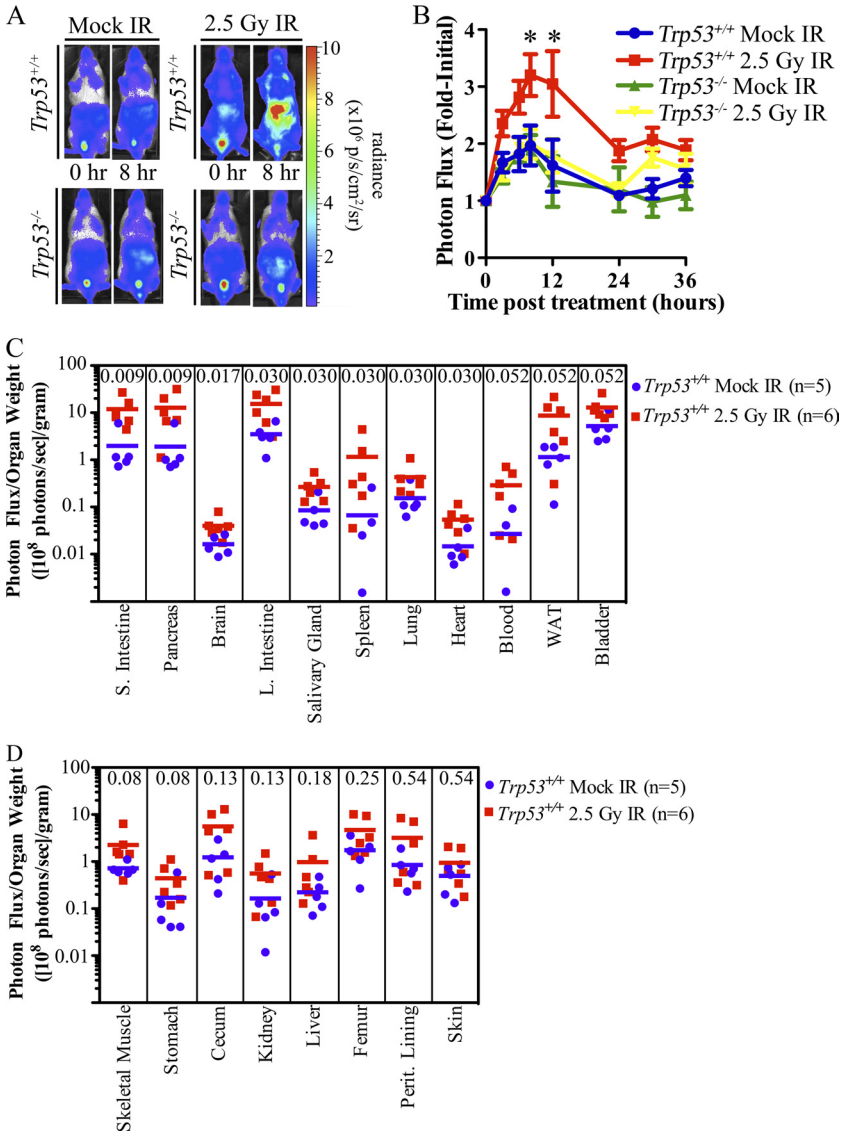

FIG. 9. IR activates the *p21* promoter in a p53-dependent manner *in vivo*. $p21^{+/FLuc}$ $Trp53^{+/+}$ and $p21^{+/FLuc}$ $Trp53^{-/-}$ mice were imaged (time zero) and then either mock irradiated or exposed to 2.5-Gy IR. Whole-body bioluminescence was determined at the indicated times posttreatment. (A) Representative images of mice; (B) bioluminescence relative to the value at time zero, displayed graphically. *, $P < 0.05$; **, $P < 0.01$ by Bonferroni posttests of a 2-way ANOVA. (C and D) $p21^{+/FLuc}$ $Trp53^{+/+}$ mice were either mock irradiated or exposed to 2.5-Gy IR, and organs were harvested 8 h later and immediately imaged. To account for variations in organ size from mouse to mouse, organ weight was determined prior to BLI. The normalized photon flux of each organ is represented as the photon flux/sample weight (photons/s/g). Individual mice (squares and circles) and the group average (bar) are shown. The Mann-Whitney U test *P* value is included in each column.

block quiescent wild-type MEFs from activating *p21* expression upon serum stimulation at a point downstream of ERK/MAPK activation. Future studies will examine *p21* promoter occupancy by ERK/MAPK-regulated transcription factors both in the presence and absence of p53.

Previous studies of *p21* expression levels in various organs of mice (at the level of endogenous protein or endogenous mRNA or in transgenic reporter mice) reported that baseline expression of *p21* is independent of p53 status (7, 27, 29, 37, 38). Of note, these observations were generally confirmed in our knock-in strain (Fig. 7 and 8), but the sensitivity of bioluminescence imaging enabled us to detect effects of loss of p53 function on expression of *p21* in mouse white adipose tissue (Fig. 3). In addition, several other organs trended toward significance. Due to the robust bioluminescence generated in our reporter mice, we were able to use microosmotic pumps to deliver a constant supply of D-luciferin to all tissues in selected experiments, which enabled protocols for imaging mice sequentially and repetitively over short or long intervals, therefore enhancing the capacity for dynamic analysis (15).

In contrast to the knock-in mice reported here, previously published studies of transgenic reporter mice carrying a *p21 LacZ* transgene (37) or a *p21* firefly luciferase (*FLuc*) transgene (29) did not accurately report *p21* promoter activity *in vivo*. For example, baseline expression of the *p21* promoter was reported to be highest in the kidney and forepaws, whereas the

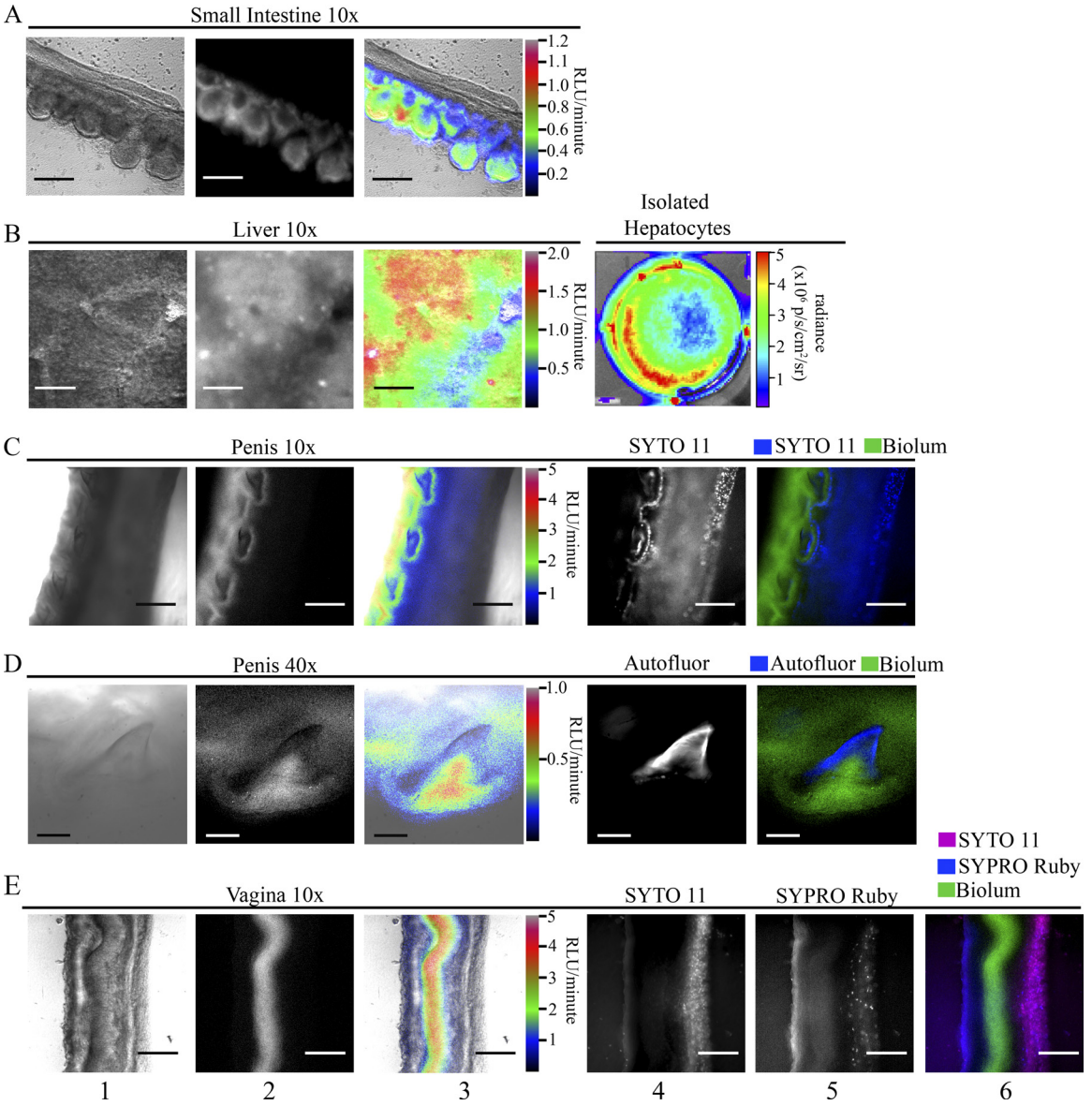

FIG. 10. Bioluminescence microscopy revealed *p21* promoter activity within organs. Tissue sections of the small intestine (A), liver (B), penis (C and D), and vagina (E) isolated from $p21^{+/FLuc}$ mice were incubated with D-luciferin-containing medium, and BLI was performed. Column 1 is the bright-field image, column 2 is the bioluminescence image, and column 3 is the pseudocolor overlay of bioluminescence on the bright field. In some cases, tissue autofluorescence (autofluor) was photographed, and tissues were stained with SYPRO ruby protein stain and/or with SYTO 11 green fluorescent nucleic acid stain. Pseudocolor overlays of fluorescence and bioluminescence images are depicted. Bars, 200 μm (10× magnifications) or 50 μm (40× magnifications).

small intestine was one of the lowest-expressing organs in a *p21 FLuc* transgenic strain (29). In contrast, in our knock-in reporter mice, the small intestine (Fig. 7 and 8) was one of the highest-expressing organs, as expected (7, 27), while kidney (Fig. 7 and 8) and forepaw (Fig. 8) were among the lowest. In the transgenic models, a truncated *p21* promoter of 2.5 kb (29) or 4.5 kb (37) drives reporter expression. In one case, the reporter strain contained 2, 3, or 22 copies of the transgene (37), whereas in the other case, the number of copies was not documented (29). Baseline expression of the *p21* promoter in the *p21 LacZ* mice was only detected in the strain with 21 copies of the transgene (37), and bioluminescence in the *p21 FLuc* transgenic strain did not exceed 10^6 photons/s (29). This is in contrast to the high baseline bioluminescence of 10^9 photons/s measured in our reporter mice under similar conditions. The observed differences between the transgenic strains and our knock-in strain are likely due, in part, to the deletion of many important regulatory regions in the truncated promoters used to create the transgenic reporter lines, as well as gene loci and related positional effects on reporter activity (4).

Given recent advances in cooled CCD cameras and our interest in tracking *p21* expression at high resolution, low-light bioluminescence microscopy allowed us to observe *p21* pro-

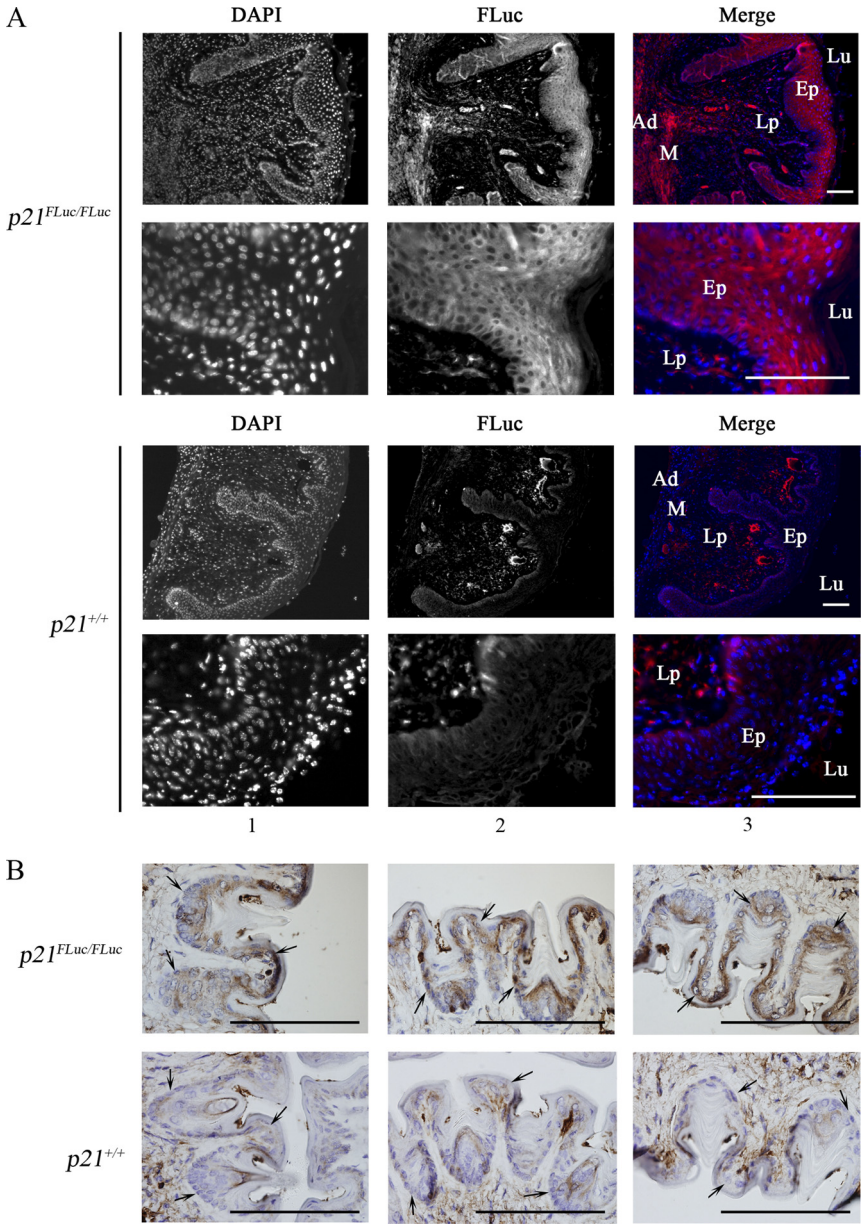

FIG. 11. Localization of FLuc protein in mouse vagina and penis. Tissue sections of vaginas (A) and penises (B) isolated from $p21^{FLuc/FLuc}$ and $p21^{+/+}$ mice were stained with antibodies specific for FLuc (red in panel A, brown in panel B) and counterstained with 4′,6-diamidino-2-phenylindole (DAPI) for nuclei (blue in panel A) and hematoxylin (B). Representative images in panel A are shown at 10× and 40× magnification and in panel B at 100× magnification. Arrows are included in panel B to mark the epithelial cells. Bars, 100 μm.

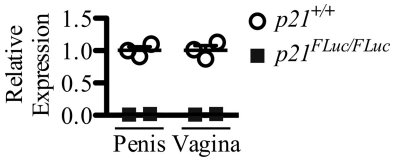

FIG. 12. Localization of *p21* mRNA in epithelial cells of vagina and penis. Epithelial cells from vaginas and penises isolated from $p21^{+/+}$ ($n = 3$ for each sex) and $p21^{FLuc/FLuc}$ ($n = 2$ for each sex) mice were isolated using laser capture microdissection. mRNA was isolated, and relative levels of *p21* mRNA were determined by normalizing to *actin* mRNA and $p21^{+/+}$ samples. Individual mice (circles and squares) and the group average (bars) are shown. Each sample was tested in triplicate, and the SEM is also shown.

moter activity within specific regions of mouse tissues. We observed *p21* promoter activity in the differentiated epithelia of various organs (penis, vagina, and small intestine) as well as in liver hepatocytes, a relatively quiescent cell population (Fig. 10). The observation of *p21* expression in differentiated epithelia of the external genitalia was novel. The ability to use microscopy to visualize *p21* expression provides an additional advantage, as bioluminescence microscopy does not require potentially cytotoxic excitation light and typically has extremely low background signals (13). The real-time nature of FLuc-based tracking of reporters in eukaryotic cells also allows serial measurements from the same region over time (16). Hence,

bioluminescence microscopy is well-suited to kinetic studies of *p21* expression in specific regions of organs not previously amenable to analysis.

In summary, we generated knock-in luciferase reporter mice in which the *p21* gene locus was targeted, and these mice will be particularly useful for elucidating more fully the many known upstream regulators of *p21* promoter activity *in vivo* and, due to the ease of bioluminescence imaging, also will be useful for characterizing novel p53-independent regulators of the *p21* promoter in living mice.

ACKNOWLEDGMENTS

We thank Jiling Song, Sofia Origanti, and Courtney Robinson for technical support during the early stages of this project. We thank Mike White for performing blastocyst injections, Chris Ryan and Emily Powell for editorial assistance, and Reece Goiffon for assistance with statistics. Shin-ichiro Imai and Cindy Brace are thanked for help in isolating and culturing primary hepatocytes. Raleigh Kladney is thanked for help with mouse perfusions. Jason Weber and Jason T. Forys are thanked for advice on experiments related to serum starving of MEFs. We thank the Alvin J. Siteman Cancer Center at Washington University School of Medicine and Barnes-Jewish Hospital for the use of the Embryonic Stem Cell Core and electroporation services. The RNAi Consortium of the Broad Institute and the Children's Discovery Institute are thanked for providing shRNAs.

This study was supported in part by grant P50 CA94056 to the Molecular Imaging Center at Washington University, by P30 NS057105 to Washington University, by NIH grant MH63140 to E.D.H., and by a DOD Prostate Cancer Research Program Training Award Grant (PC101951) to K.L.T. H.P.-W. is a Research Professor of the American Cancer Society. The Siteman Cancer Center is supported in part by an NCI Cancer Center Support Grant (P30 CA91842).

REFERENCES

1. **Abbas, T., and A. Dutta.** 2009. p21 in cancer: intricate networks and multiple activities. Nat. Rev. Cancer **9:**400–414.
2. **Abramoff, M. D., P. J. Magelhaes, and S. J. Ram.** 2004. Image processing with ImageJ. Biophotonics Int. **11:**36–42.
3. **Abukhdeir, A. M., and B. H. Park.** 2008. p21 and p27: roles in carcinogenesis and drug resistance. Expert Rev. Mol. Med. **10:**e19.
4. **al-Shawi, R., J. Kinnaird, J. Burke, and J. O. Bishop.** 1990. Expression of a foreign gene in a line of transgenic mice is modulated by a chromosomal position effect. Mol. Cell. Biol. **10:**1192–1198.
5. **Besson, A., S. F. Dowdy, and J. M. Roberts.** 2008. CDK inhibitors: cell cycle regulators and beyond. Dev. Cell **14:**159–169.
6. **Bottazzi, M. E., X. Zhu, R. M. Bohmer, and R. K. Assoian.** 1999. Regulation of $p21^{Cip1}$ expression by growth factors and the extracellular matrix reveals a role for transient ERK activity in G_1 phase. J. Cell Biol. **146:**1255–1264.
7. **Bouvard, V., et al.** 2000. Tissue and cell-specific expression of the p53-target genes: bax, fas, mdm2 and waf1/p21, before and following ionising irradiation in mice. Oncogene **19:**649–660.
8. **Cazzalini, O., et al.** 2010. $p21^{CDKN1A}$ participates in base excision repair by regulating the activity of poly(ADP-ribose) polymerase-1. DNA Repair (Amst.) **9:**627–635.
9. **Cheng, M., et al.** 1999. The $p21^{Cip1}$ and $p27^{Kip1}$ CDK 'inhibitors' are essential activators of cyclin D-dependent kinases in murine fibroblasts. EMBO J. **18:**1571–1583.
10. **Dothager, R. S., et al.** 2009. Advances in bioluminescence imaging of live animal models. Curr. Opin. Biotechnol. **20:**45–53.
11. **el-Deiry, W. S.** 1998. Regulation of p53 downstream genes. Semin. Cancer Biol. **8:**345–357.
12. **Ferguson, A. M., L. S. White, P. J. Donovan, and H. Piwnica-Worms.** 2005. Normal cell cycle and checkpoint responses in mice and cells lacking Cdc25B and Cdc25C protein phosphatases. Mol. Cell. Biol. **25:**2853–2860.
13. **Flentie, K. N., et al.** 2008. Stably integrated luxCDABE for assessment of Salmonella invasion kinetics. Mol. Imaging **7:**222–233.
14. **Gartel, A. L., and A. L. Tyner.** 1999. Transcriptional regulation of the $p21^{WAF1/CIP1}$ gene. Exp. Cell. Res. **246:**280–289.
15. **Gross, S., U. Abraham, J. L. Prior, E. D. Herzog, and D. Piwnica-Worms.** 2007. Continuous delivery of D-luciferin by implanted micro-osmotic pumps enables true real-time bioluminescence imaging of luciferase activity in vivo. Mol. Imaging **6:**121–130.
16. **Gross, S., and D. Piwnica-Worms.** 2005. Real-time imaging of ligand-induced IKK activation in intact cells and in living mice. Nat. Methods **2:**607–614.
17. **Gross, S., and D. Piwnica-Worms.** 2005. Spying on cancer: molecular imaging in vivo with genetically encoded reporters. Cancer Cell **7:**5–15.
18. **Humphries, M. J., et al.** 2006. Suppression of apoptosis in the protein kinase CΔ null mouse in vivo. J. Biol. Chem. **281:**9728–9737.
19. **Klaunig, J. E., et al.** 1981. Mouse liver cell culture. I. Hepatocyte isolation. In Vitro **17:**913–925.
20. **Klaunig, J. E., P. J. Goldblatt, D. E. Hinton, M. M. Lipsky, and B. F. Trump.** 1981. Mouse liver cell culture. II. Primary culture. In Vitro **17:**926–934.
21. **Klerk, C. P., et al.** 2007. Validity of bioluminescence measurements for noninvasive in vivo imaging of tumor load in small animals. Biotechniques **43**(1 Suppl.):7–13.
22. **LaBaer, J., et al.** 1997. New functional activities for the p21 family of CDK inhibitors. Genes Dev. **11:**847–862.
23. **Lee, S., and D. M. Helfman.** 2004. Cytoplasmic $p21^{Cip1}$ is involved in Ras-induced inhibition of the ROCK/LIMK/cofilin pathway. J. Biol. Chem. **279:**1885–1891.
24. **Lee, W. J., et al.** 2006. Organ-specific gene expressions in C57BL/6 mice after exposure to low-dose radiation. Radiat. Res. **165:**562–569.
25. **Liu, Y., J. L. Martindale, M. Gorospe, and N. J. Holbrook.** 1996. Regulation of $p21^{WAF1/CIP1}$ expression through mitogen-activated protein kinase signaling pathway. Cancer Res. **56:**31–35.
26. **Luo, Y., J. Hurwitz, and J. Massague.** 1995. Cell-cycle inhibition by independent CDK and PCNA binding domains in $p21^{Cip1}$. Nature **375:**159–161.
27. **Macleod, K. F., et al.** 1995. p53-dependent and independent expression of p21 during cell growth, differentiation, and DNA damage. Genes Dev. **9:**935–944.
28. **National Research Council.** 1996. Guide for the care and use of laboratory animals. National Academy Press, Washington, DC.
29. **Ohtani, N., et al.** 2007. Visualizing the dynamics of $p21^{Waf1/Cip1}$ cyclin-dependent kinase inhibitor expression in living animals. Proc. Natl. Acad. Sci. U. S. A. **104:**15034–15039.
30. **Parker, S. B., et al.** 1995. p53-independent expression of $p21^{Cip1}$ in muscle and other terminally differentiating cells. Science **267:**1024–1027.
31. **Sarbassov, D. D., D. A. Guertin, S. M. Ali, and D. M. Sabatini.** 2005. Phosphorylation and regulation of Akt/PKB by the rictor-mTOR complex. Science **307:**1098–1101.
32. **Sato, T., et al.** 2009. Single Lgr5 stem cells build crypt-villus structures in vitro without a mesenchymal niche. Nature **459:**262–265.
33. **Sherr, C. J., and R. A. DePinho.** 2000. Cellular senescence: mitotic clock or culture shock? Cell **102:**407–410.
34. **Sherr, C. J., and J. M. Roberts.** 1999. CDK inhibitors: positive and negative regulators of G_1-phase progression. Genes Dev. **13:**1501–1512.
35. **Sherr, C. J., and J. M. Roberts.** 1995. Inhibitors of mammalian G_1 cyclin-dependent kinases. Genes Dev. **9:**1149–1163.
36. **Stewart, S. A., et al.** 2003. Lentivirus-delivered stable gene silencing by RNAi in primary cells. RNA **9:**493–501.
37. **Vasey, D. B., C. R. Wolf, T. MacArtney, K. Brown, and C. B. Whitelaw.** 2008. p21-LacZ reporter mice reflect p53-dependent toxic insult. Toxicol. Appl. Pharmacol. **227:**440–450.
38. **Wilson, J. W., D. M. Pritchard, J. A. Hickman, and C. S. Potten.** 1998. Radiation-induced p53 and $p21^{WAF-1/CIP1}$ expression in the murine intestinal epithelium: apoptosis and cell cycle arrest. Am. J. Pathol. **153:**899–909.